

P1.9 TWO-WAY (HOUR-MONTH) TIME-SECTION PLOTS AS A TOOL FOR CLIMATOLOGICAL VISUALIZATION AND SUMMARIZATION

Charles J. Fisk *
NAWCWPNS-Point Mugu, CA

1. INTRODUCTION

Diurnal and seasonal variability in meteorological conditions that can potentially influence the conduct of human activities is a fact of nature for every locality on Planet Earth. This variability and the uncertainty it entails necessitates weather forecasts, but since forecast accuracy usually decays significantly for periods of interest beyond a few weeks time, climatology must frequently serve as the principal planning and decision-aid tool in long-range applications. In years past, climatological data often appeared in the form of tabular summaries, ordered by month, time of day, wind direction, or some other category. Not infrequently, the sheer volume of the compilations necessitated that presentations be confined to an hourly subset (e.g., every third-hour).

The advent of desktop computing power and the availability of powerful data analysis and visualization software, both of these fairly recent developments, makes it readily feasible to transform and condense multiple tabular climatological summaries into concise single-page graphical layouts that give comprehensive visual feel for the seasonal and diurnal variations of a particular variable. The ultimate purpose can be operational or purely descriptive, but in either case, the information is usually more effectively conveyed in visual form. In addition, visualization products lend themselves to effective presentation on the web, the latter a comparatively new development in itself.

The purpose of the following is to illustrate the use of two-way (hour-month) time-section plots as a means of visualizing single-station climatological data, a presentation mode certainly not unknown but not believed to be widely used. With this technique, month of the year comprises one axis, hour of the day the other. Upon the grid, variables such as temperature, frequency of VFR, fog, or high winds are contoured. Off-hour data not represented in original tabular form can be estimated using the same smoothing and interpolation techniques available for spatial analysis. Multiple contours can be created to represent additional variables, as can color schemes, the latter significantly enhancing graph appearances. In addition, sunrise and sunset demarcations can be overlain, lending an additional physical perspective to the parameter s climatological variation.

Sample charts depicting diurnal/monthly variation in Flying Weather conditions (combinations of ceiling and visibility), temperature and humidity, adverse weather

conditions (Fog, Blowing Sand/Dust, Thunderstorm Activity, High Winds, and Precipitation) are presented. Also included are plots of derived climatological variables, such as mean vector winds vs. constancy, or percent of time with overcast/broken sky conditions vs. median ceiling heights. In nearly all cases, the charts are constructed utilizing monthly, every-third hour cross-tabulated data (either occurrence frequencies or statistical averages) from the NOAA National Climatic Data Center ISMCS Version 3.0 CD-ROM product (1995).

2. SAMPLE CHART CREATION (FLYING WEATHER APPLICATION)

Figures 1 and 2 below are sample two-way climatological time-section plots depicting the percentage frequencies of Visual-Flight-Rules (VFR) and Precision Approach Radar (PAR) conditions, respectively, at Point Mugu, CA (34.1 N, 119.1 W, elev. 13 ft), a U. S. Naval facility about 50 miles WNW of Los Angeles, along the Pacific Ocean.

The original data were in the form of every-third-hour percent occurrence frequencies, by month, for 0100, 0400, 0700, 1000, 1300, 1600, 1900, and 2200 LST) - in all, some 96 pieces of information. Since the data were to be contoured and the time-variables on each axis were circular, to reduce adverse wrap-around effects where the contours would intersect chart edges (i.e., insuring that a given contour value ran off opposite margins of a given chart at approximately the same ordinate or abscissa value), duplicate parameter values with 12-month or 24-hour position offset values were created and incorporated into the internal data array. This duplication or padding was done several time-units deep , enlarging the total number of data elements to 216. The month of January, for example, in addition to its normal ordinal position value at $y=1.5$, had a duplicate at $y=13.5$, the latter outside the range of the chart as it would be presented, but part of the contour creation process near the chart s upper edge. In like fashion, the 0100 LST hour, in addition to its normal $x=1.0$ position, had a duplicate at $x=25.0$, also outside the range of the chart, but part of the same internal contour shaping process, this time along the chart s right edge. With padding complete, the data were kriged, smoothed, cropped, contoured, and colored.

The sunrise/sunset demarcation curves were derived from downloaded data from The U.S. Naval Observatory s Sun or Moon-rise/Set Table for One Year online site. The latitude/longitude coordinate for Point

* Corresponding author address: Charles J. Fisk,
NAWCWPNS, Point Mugu, CA. 93042: e-mail:
charles.fisk@navy.mil

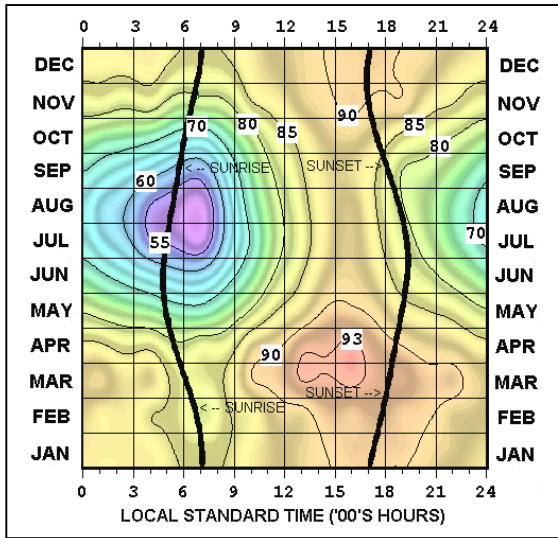


Figure 1. Percent of Time with Visual Flight Rules (VFR) Conditions at Point Mugu, CA (Ceilings >= 1000 ft. and Visibilities >= 3 mi.)

Mugu was specified, along with its time zone, and a sunrise/sunset table was generated for each day of the year that could be saved as a text file. Application of additional programming and graphical software capabilities converted the data into the overlays that appear in the figure.

From Figure 1, it is apparent at first glance what time of year/time of day is most favorable for VFR conditions (afternoons in late March/early April, with a better than 93% incidence, climatologically). Such optimal period identification would not be as quick via trial-and-error tabular inspection(s). The chart also gives an all-inclusive picture on the seasonal and diurnal variation of VFR, probably an unattainable result in such rapid fashion by other means.

Figure 2 depicts the climatological incidence of Point Mugu Precision Approach Radar (PAR) conditions, a highly restrictive visibility and ceiling condition for aircraft operations. Interpretation is in the complementary sense relative to Figure 1 (i.e., higher magnitude contours indicate less favorable times of the year regarding PAR). The 7 percent or greater contour region, confined primarily to late-September just before sunrise, reflects to some extent the lengthening nights at this time of year and the consequent greater tendency for fog formation in the still relatively moist lower atmosphere.

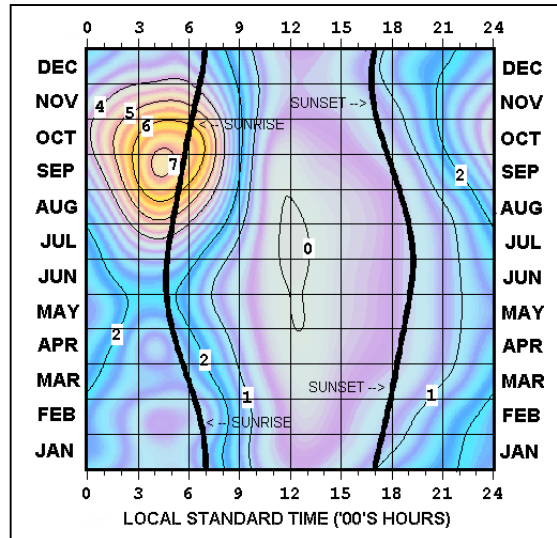


Figure 2. Percent of Time with Precision Approach Radar (PAR) Conditions at Point Mugu, CA (Ceilings < 100 ft. and/or Visibilities < 1/2 mi.)

2.1 TWO-WAY TEMPERATURE/HUMIDITY CHARTS

Figure 3 is a sample chart depicting the diurnal/seasonal variation in mean temperature and humidity for a sample station, in this case Bahrain International Airport, along the Persian Gulf.

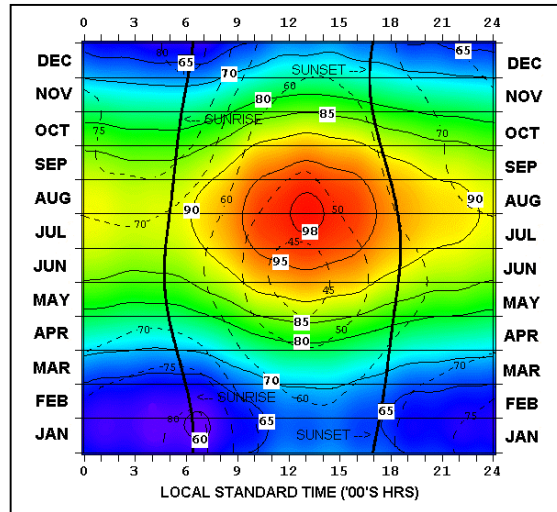


Figure 3. Mean Temperature (Solid Lines/Color) and Relative Humidity (Dashed Lines) at Bahrain International Airport.

The fact that temperatures are warm in Bahrain in July is certainly not a revelatory feature of the graph, but superposition of the dashed humidity contours, indicating that conditions can be very warm AND sultry (e.g., mean mid-July temperature of 98 F just after noon combined with relative humidities of 45%) is useful additional information. In this particular application, it would have also been possible to substitute dewpoint contours in lieu of relative humidity ones.

2.2 TWO-WAY FOG FREQUENCY CHARTS

Two-way charts can also prove useful in identifying on a diurnal and seasonal basis the most unfavorable or favorable times for a number of other types of visibility-restricted conditions. One of these is Fog, and the following three charts depict incidence at three

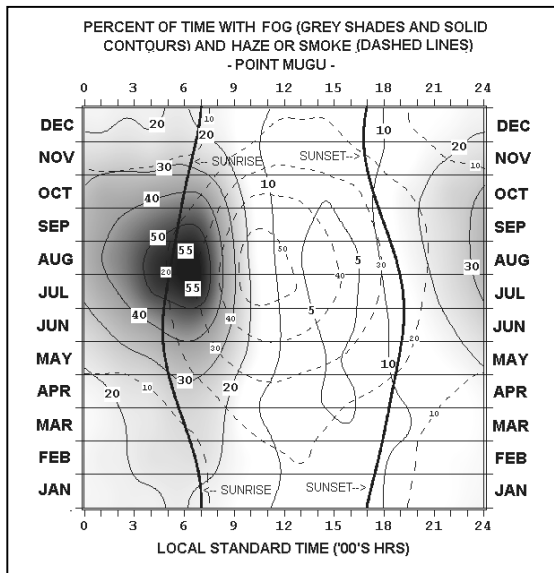


Figure 4. Percent Incidence of Fog (Solid Lines/Color) and Haze/Smoke (Dashed Lines) at Point Mugu, CA

relatively fog-prone sites: Point Mugu, CA. (see Figure 4); St. John s, Newfoundland (the foggiest city in Canada- see Figure 5); and London, U.K. (Gatwick Airport- see Figure 6). Additional contour lines (dashed) are added for Haze and Smoke. Comparing inter-station contour topographies, of course, can be part of a decision-making process in itself, although the charts displayed here are for demonstrative and descriptive purposes only.

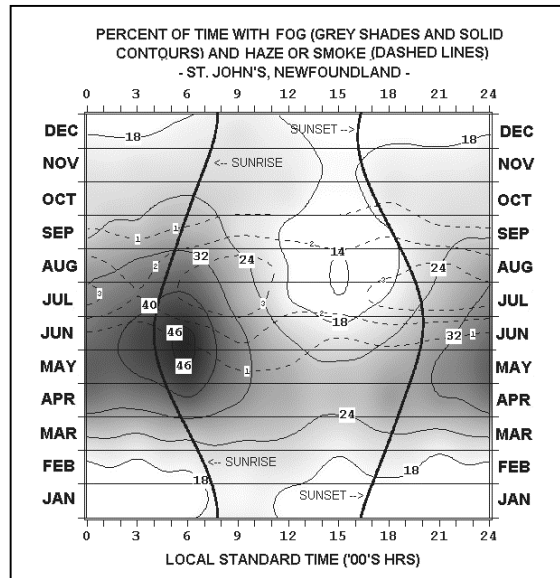


Figure 5. Percent Incidence of Fog (Solid Lines/Color) and Haze/Smoke (Dashed Lines) at St. John s Newfoundland, Canada

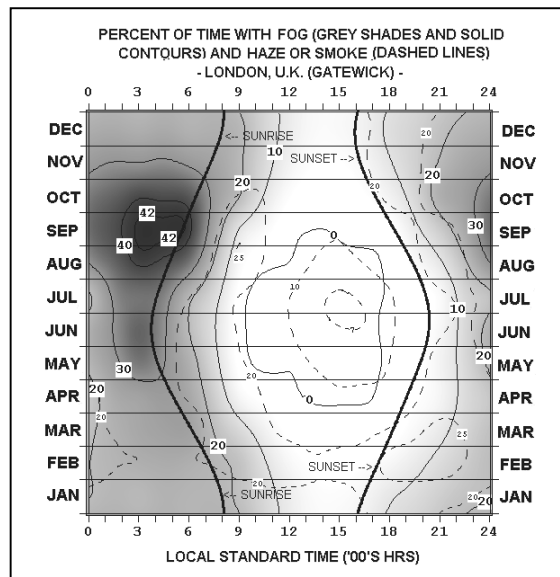


Figure 6. Percent Incidence of Fog (Solid Lines/Color) and Haze/Smoke (Dashed Lines) at London, U.K. (Gatwick).

The three stations all show varying times seasons of year for their relative maxima — Point Mugu in July-August, St. John s in May-June, and London in September. Also, on a diurnal basis, London s September maximum seems to be more of a pre-sunrise phenomenon, St. John s apparent for the hours immediately after sunrise. While London s contour maximum (42%) is comparable in magnitude to St. John s (46%), Fog incidence for London is zero for most late morning and early afternoon hours during the months April through August. St. John s minimum contour, in contrast, is a considerably higher 14%, for late July and August for the mid-afternoon hours. Point Mugu s seasonal maximum (55%) and minimum (5%) occur in the same month (August), although the latter figure also applies for a number of other months (April-September) for the same mid-afternoon hours. Conditions are also considerably more hazy at Pt. Mugu, especially in summer, a trademark of Southern California weather at this season near the coasts. The 50% contour is evident for the morning hours up to about noon, the 40% contour extending well into the afternoon. In contrast, the highest magnitude Haze/Smoke contours for London and St. John s are just 25 % and 3 %, respectively.

2.3 TWO-WAY BLOWING SAND/DUST FREQUENCY CHARTS

Another weather condition type that can affect activities and operations is Blowing Sand and Dust . and two sample charts are provided below as illustrative examples.

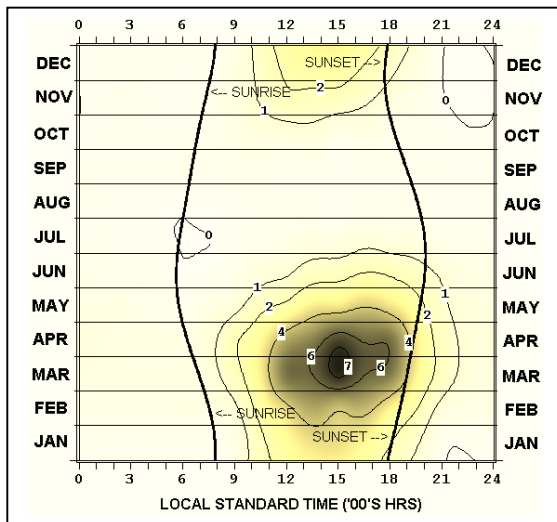


Figure 7. Percent Incidence of Blowing Sand and Dust at Lubbock, Texas.

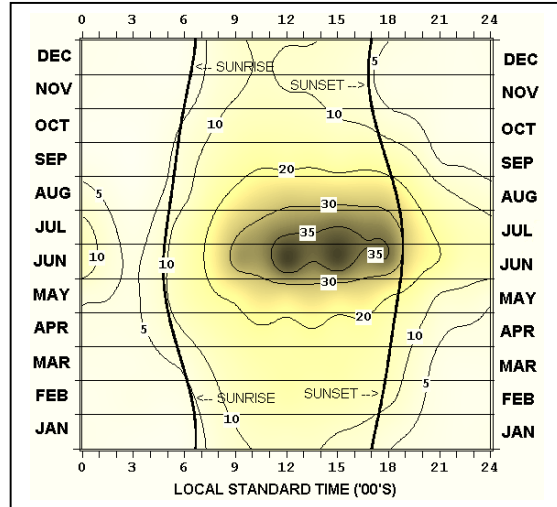


Figure 8. Percent Incidence of Blowing Sand and Dust at Kuwait City, Kuwait.

Figures 7 and 8 show the percent incidence of Blowing Sand and Dust for Lubbock, Texas (one of the more dust-prone stations in the continental U. S.) and Kuwait City, Kuwait (probably more sand-prone than dust-prone), respectively. Lubbock exhibits a March-April maximum (7% contour) for the mid-afternoon hours. Kuwait City, in contrast, shows a much more pronounced maximum (35 % contour), essentially covering June and early July from noon until just before sunset, predominantly reflecting occurrences of the Shamal , the strong Northwesterly wind regime that prevails at this time of year.

2.4 TWO-WAY THUNDERSTORM FREQUENCY CHARTS

Yet another weather condition type whose seasonal and diurnal variation is of interest and importance is the thunderstorm. The associated rain, of course, can affect activities and operations, but aside from the precipitation, the possibility of lightning discharges can also be of concern. Figures 9 through 12 show the seasonal/diurnal incidence of thunderstorm activity at four stations: Fort Myers, Florida; North Platte, Nebraska; Calcutta, India, and Rio de Janeiro, Brazil, respectively. All these stations show somewhat differing topographies of thunderstorm incidence.

Fort Meyers (see Figure 9), one of the more thunderstorm-frequent stations in the United States shows a pronounced maximum contour (23 %) confined mostly to the late afternoons in July and August. North Platte (see Figure 10), in contrast, exhibits a noticeably more nocturnal pattern, although the maximum contour (5 %) is considerably lower in magnitude. Calcutta shows a fairly large area of high contour magnitudes,

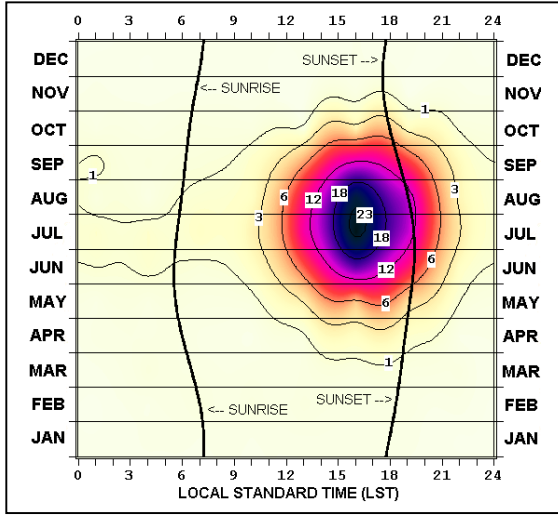


Figure 9. Percent Incidence of Thunderstorm Activity at Fort Myers, Florida

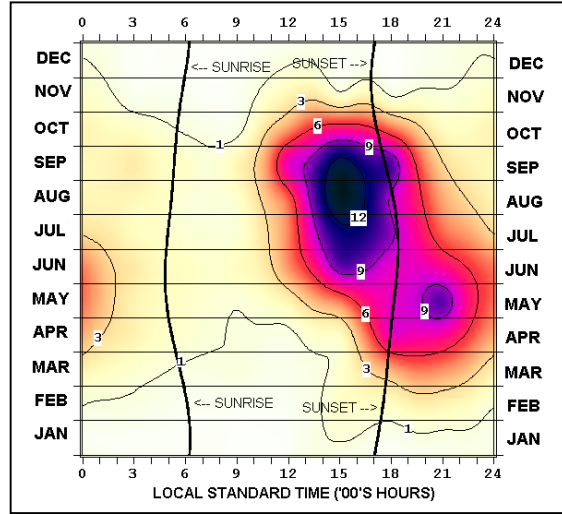


Figure 11. Percent Incidence of Thunderstorm Activity at Calcutta, India

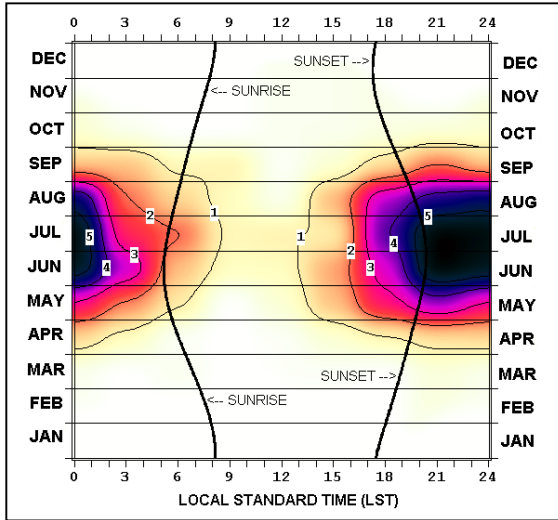


Figure 10. Percent Incidence of Thunderstorm Activity at North Platte, Nebraska

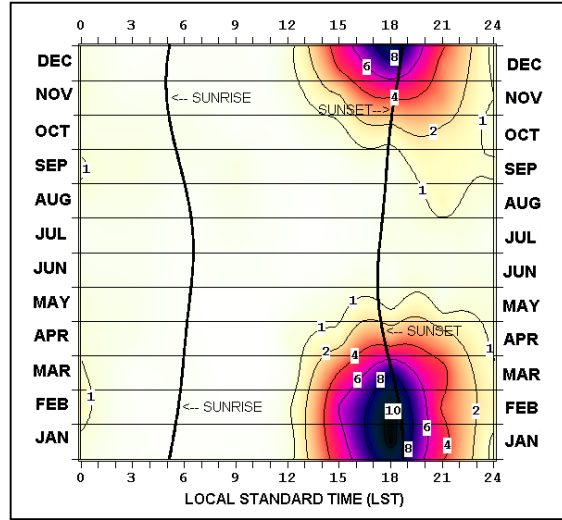


Figure 12. Percent Incidence of Thunderstorm Activity at Rio de Janeiro, Brazil

associated mostly with the Asian Monsoon, but there is also a noticeable post-sunset secondary maximum for May, a pre-monsoonal month. Climatologically, the Monsoon at Calcutta is considered to run from mid-June to mid-August [Ghosh, 2000].

Thunderstorm activity in Rio de Janeiro exhibits its climatological maximum over late December to late March (Austral Summer) in the late afternoon to early afternoon, reflecting diurnal heating of the humid, unstable equatorial air mass typically predominant over the area at this season [Trewartha and Horn, 1980].

2.5 TWO-WAY HIGH WINDS CHARTS

Figure 13 depicts the diurnal/seasonal incidence of sustained wind speeds at or above 17 knots for NOAA Buoy 46025, an anchored buoy about 33 nautical miles WSW of Santa Monica, CA. This speed threshold has operational significance in that winds at or above 17 knots are known to adversely affect small surface craft. Buoy 46025 wind data were available for each hour of the day, but were reduced to an every-third hour format starting with 0100 LST.

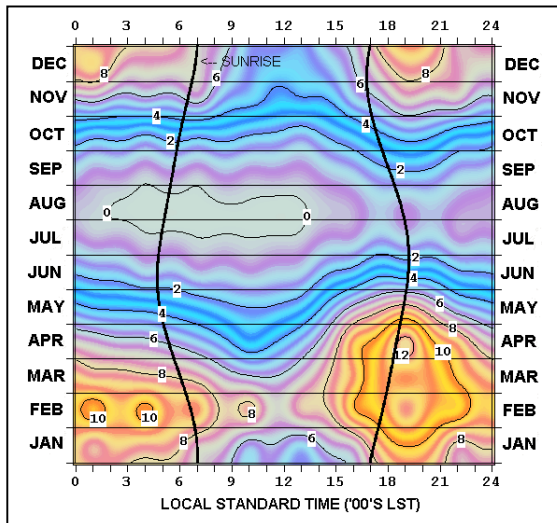


Figure 13. Percent of Time with Winds ≥ 17 knots at NOAA Buoy 46025 (33.7 N, 119.1 W)

From the chart, to avoid 17 knot winds to the maximum degree (i.e., the 0% contour-enclosed region), small-craft activity in daytime should be confined to late-July and August from sunrise to approximately 1300 LST. Most unfavorable daylight times, in contrast, are principally for the months February-April in the late afternoon; a 12% contour is noted for April just after sunset.

Buoy 46025 is close enough to shore so that the diurnal influence on high wind frequency, predominately a land-induced feature, is still evident.

2.6 TWO-WAY PRECIPITATION CHARTS

As a sample two-way precipitation chart, Figure 14 depicts the diurnal/seasonal frequencies of rain/drizzle (solid line) and snow/sleet at Whidbey Island, Washington (48.3 N, 122.7 W), an island-based naval facility in Puget Sound about 50 miles northwest of Seattle.

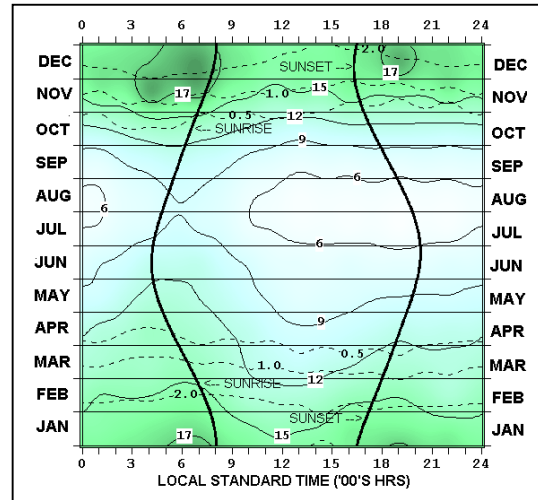


Figure 14. Percent of Time with Rain/Drizzle (solid) and Snow/Sleet (dashed) at Whidbey Island, Washington

Whidbey Island clearly has a cold-season maximum in precipitation incidence with evidence of a slight nocturnal propensity for rain/drizzle at that time as well; the 17% rain/drizzle contour maxima are confined almost exclusively to the November and December pre-sunrise and post-sunset hours, respectively.

The snow/sleet isolines, in contrast, run more parallel to the calendar month demarcation lines, although the area enclosed by the 2% contours, appears slightly wider for the pre-sunrise hours of December, January, and February.

Minimum precipitation frequency, delineated by the area within the 6% contour, is evident for July-August from the hours 1000-1100 LST through 0100 LST.

2.7 TWO-WAY CHARTS USING DERIVED DATA — MEAN VECTOR WIND/CONSTANCY CHARTS

Another application of two-way time-section plots is visualization of meteorological parameters that originally didn't appear explicitly in published form but were instead derived from data that did.

One example is the depiction of estimated mean vector wind statistics from joint wind direction/speed frequency tabulations. In the NOAA National Climatic Data Center ISMCS Version 3.0 CD-ROM product, for instance, many of the stations' wind data appear as every third-hour cross-tabulations of sixteen-point compass directions vs. Beaufort Scale speed

occurrences, by month. Such data are frequently used to construct wind rose diagrams, and in this instance some 96 wind roses are possible.

Utilizing the direction/speed categories joint means as synthetic observations weighted by their bin frequencies, mean vector wind statistics could also be estimated for the 96 hours along with interpolated figures for the other 192 hours that were not included in the original every-third-hour selection. Most importantly, this mean vector wind information could be presented on a single page.

To illustrate the calculation process, the two-way northwesterly wind direction/seven-to-ten-knot wind speed category for example, would have an assigned synthetic vector magnitude of 315 degrees @ 8.5 knots, the derived east-west, or *u* component, and north-south, or *v* component +6.01 and -6.01 knots, respectively. In analogous fashion, all the other possible two-way wind direction/wind speed categories would be assigned synthetic joint magnitudes along with *u*-component and *v*-component derivations. Then, using the bin frequencies as weights, mean scalar speed, mean *u*, and mean *v* statistics would be calculated for each of the 96 hours. From these, off-hour mean scalar speed, *u*, and *v* statistics for the 192 hours that were not part of the original every-third-hour interpolation would be estimated from cubic-spline interpolation of the calculated every-third-hour mean scalar speeds, *u* *s* and *v* *s*. Next, mean vector wind directions and speeds for all the hour/monthly combinations (288) would be constructed using the $\arctan(v/u)$ and $\sqrt{v^2+u^2}$ functions, respectively; constancy statistics were calculated using ratios of mean vector wind speeds to mean scalar speeds.

Finally, the mean vector direction, speed, and vector wind constancy statistics were then graphed onto a single page layout, providing a comprehensive picture of mean vector wind character (direction, speed, and constancy), diurnally and seasonally.

As a first sample, Figure 15 is a mean vector wind/constancy chart for Point Mugu, CA., based on monthly every-third-hour cross-tabulated data. The mean vector (or resultant) winds are depicted as arrows, oriented in the direction of flow, and their lengths are proportional to their magnitudes. For continuity purposes, the 0000 LST vectors near the left-edge of the graph are repeated as 2400 LST vectors near the right-edge. Vector wind constancy, the ratio of the mean vector wind speed to the mean scalar mean wind speed, is depicted by the color scheme. Dark blue areas indicate the lowest wind constancies, red areas the highest.

From the chart, the most prominent feature is the area of relatively high magnitude/high constancy southwesterly to westerly mean vectors in the mid-morning to late afternoon of spring, summer, and fall, reflecting the sea breeze. The vectors exhibit a clockwise, coriolis-force turning from morning to afternoon, showing the highest constancy maxima (90 or higher — depicted by the brightest red areas) for the mid-to-late afternoon hours of May to August. The general red region is also widest for June-August,

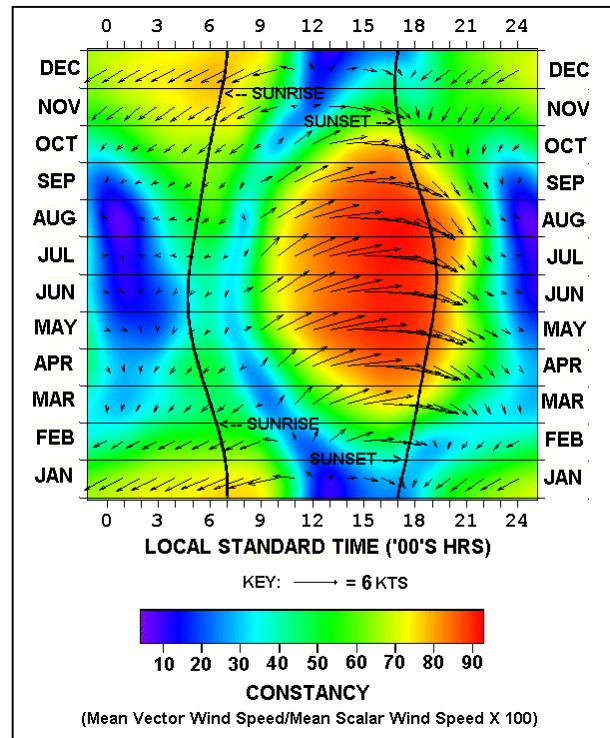


Figure 15. Mean Vector Wind/Constancy Chart for Point Mugu, CA.

indicative that the sea breeze commences earlier in the day during these months. Another feature is the relatively persistent (yellow to orange areas) of northeasterly vectors for November through January, associated with Santa Ana (offshore flow episodes).

The constancy minima areas reflect the light and variable wind character of the majority of the post-midnight to pre-sunrise hours that encompass May to September. They also identify offshore-flow/onshore-flow transitional periods, exemplified most prominently by the relatively extensive blue areas covering the early afternoon hours for December and January, and to a lesser extent by the post-sunrise, bluish ring to the left of the red maxima region, visible almost continuously from March to October, inclusive.

An inevitable question concerning the use of mean vector wind statistics generated in this manner is the level of statistical accuracy degradation. Fisk [1999], using a 1973-1992 test sample of originally observed 36-point compass, nearest-knot hourly wind data, for Pt. Mugu, created a synthetic set of sixteen-point compass Beaufort scale observations derived from the same 20 years' data set and compared the mean vector wind statistics, original vs. synthetic. Results showed only a slight degradation in statistical precision, the most significant relative errors encountered for those off-hours that corresponded to diurnal transition periods. Visualized as two separate black and white charts, one depicting mean vector wind information derived from the

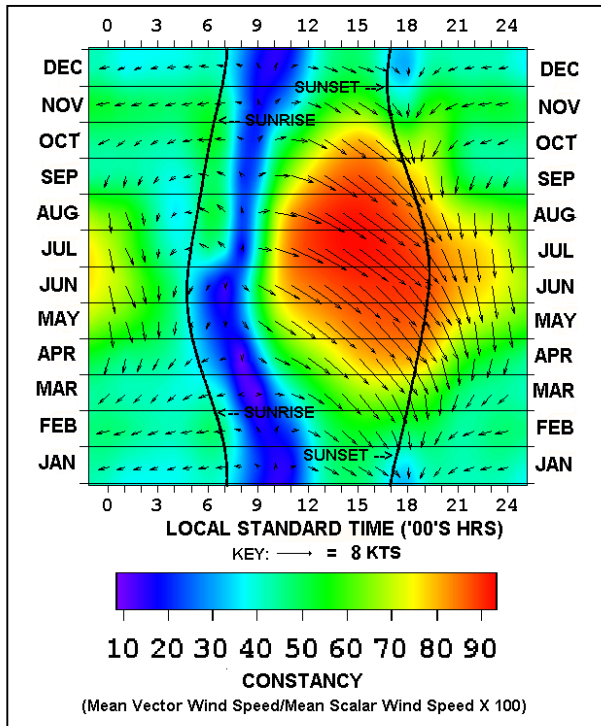


Figure 16. Mean Vector Wind/Constancy Chart for Bakersfield, CA.

original hourly wind observations, the other from the synthetic data (contours instead of colors for the constancies), the discrepancies were scarcely noticeable and had no effect on interpretation of the essential features of the station's diurnal/seasonal wind character.

Figure 16 shows the diurnal/monthly mean vector wind character for Bakersfield, California, near the south end of the San Joaquin Valley. Again, the mean vector wind statistics are derived from every-third-hour cross-tabulated data. The blue-colored post-sunrise diurnal transition period is even more prominent than it was for Pt. Mugu, and is clearly evident for all months of the year. There is also a similarly situated high constancy area, reflecting Bakersfield's own (northwesterly) sea breeze, enhanced by gradients resulting from the thermal low that typically forms in the California Central Valley during the warmer months [Keislar, et. al., 2003].

In a final example, Figure 17 shows the mean vector wind/constancy chart for Diego Garcia (7.30 S, 72.40 E), a small British island dependency just south of the equator in the Indian Ocean. In great contrast with the previous two figures, there is almost no diurnal variation in mean vector wind orientation and constancy; what variation that is present is predominantly month-to-month (note also the slight variation in sunrise/sunset times through the course of the year). The high constancy area (figures mostly in the 80 s), covering essentially May-September, reflects the predominance

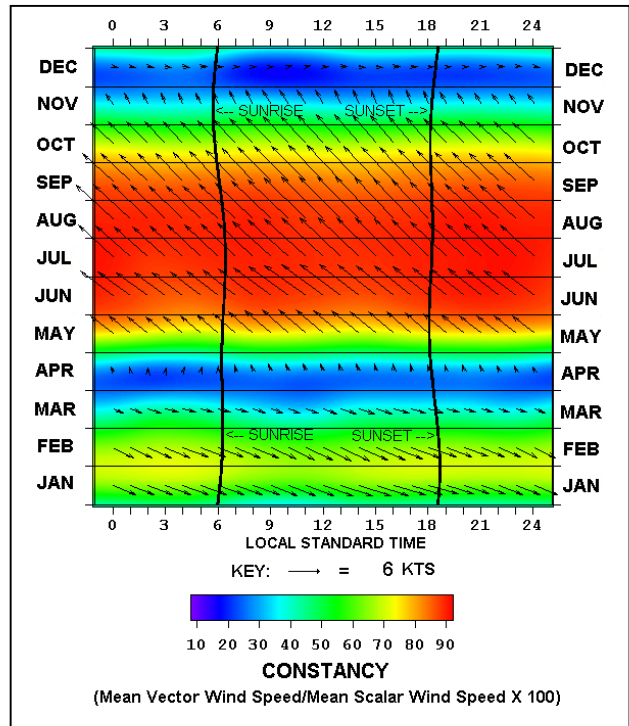


Figure 17. Mean Vector Wind/Constancy Chart for Diego Garcia

of the Southeast Trade winds at these times. Northwesterly vectors prevail in January and February, although the constancy values are lower, in the 50 s and 60 s, as depicted by the greenish shadings. The other months, especially April and December, are essentially transitional periods.

In areas on a chart where constancy magnitudes are very high, one might infer that prevailing wind directions are very similar to the orientations shown by the mean vector wind arrows. To investigate this association statistically, Fisk [2002] analyzed the 1973-1992 relationships between Point Mugu, CA. mean vector wind constancy magnitudes and percent inclusion of individual wind direction observations within a prescribed bandwidth centered about the resultant direction. The implicit assumption, of course, was that the Pt. Mugu constancy/percent-inclusion relationships would be representative of those found for other first-order stations. Figure 18 shows the associations for the plus or minus 10-degree bandwidth selection, an interval spread similar to that for the sixteen-point compass scheme (plus or minus 11.25 degrees). The orientation of the points is fitted to a LOWESS function, a smoothed locally weighted polynomial regression model. An easily discernable positive dependence of the percent inclusion vs. constancy magnitude is evident, the slope of the curve accelerating steeply upward beyond the 75 constancy level. Percent inclusion figures are as high as 50% to 60% at the highest constancy levels.

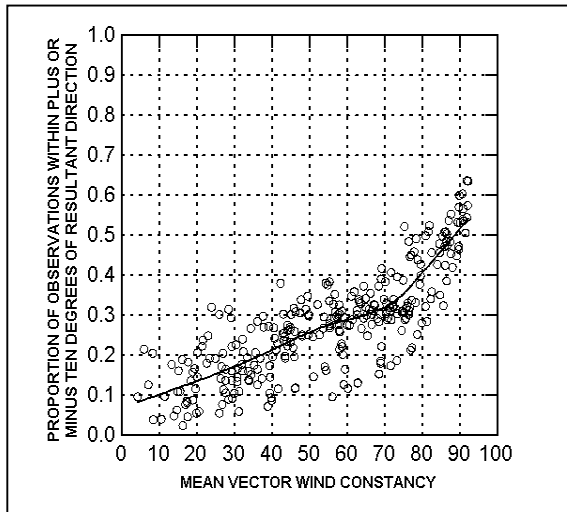


Figure 18. Percent of Individual Wind Direction Observations within Plus or Minus Ten Degrees of Climatological Mean Vector Wind Directions, as Function of Constancy Magnitudes — Point Mugu, CA., Hourly Wind Data (1973-1992).

2.8 TWO-WAY CHARTS USING DERIVED DATA — PERCENT OF TIME WITH CEILINGS/MEDIAN CEILING HEIGHTS CHARTS

A second type of derived data chart is the percent of time with broken or overcast sky conditions (i.e., cloud ceilings) vs. median ceiling heights.

In the NCDC ISMCS CD-ROM product, percent of time with broken or overcast sky conditions data were explicitly presented, by month, for every third-hour, but median ceiling heights had to be derived from two-way tables containing cumulative percent categories of both ceiling height (including the unlimited category) and visibility. In this instance, using frequency tabulations in the ≥ 0 miles visibility category (all visibilities), median ceiling height was determined by linearly interpolating a 50th percentile ceiling height for a subset of the height data after the unlimited ceilings category frequency magnitude was subtracted out.

Figure 19 is a plot of Whidbey Island percentage frequencies with ceilings (i.e., Broken or Overcast sky conditions) and median ceiling heights. Evident from the chart is an inverse relationship between percent incidence and median heights, in other words, higher (lower) median ceiling heights are associated with lower (higher) percent incidence; actual linear correlation for the original 96 monthly, every-third-hour joint statistics is -0.582 .

Percent frequency of broken or overcast sky conditions is at a maximum in December and January, the 78% contours extending diurnally from around sunrise to 1400 LST, the minimum area (40% contours) encompassing mid-July and most of August for the hours 1500 LST to 2300 LST. Median heights are at a minimum (2200-foot dashed contour) for a confined

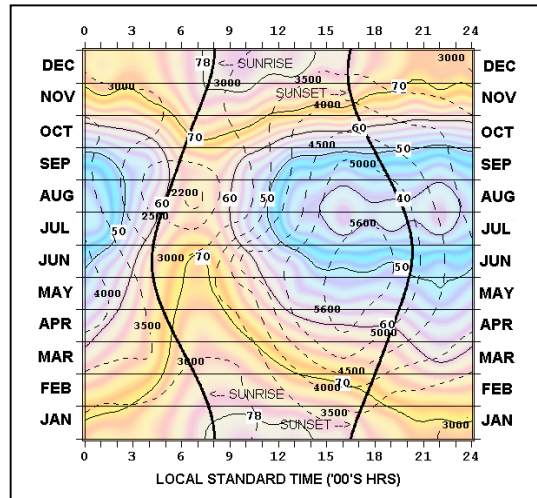


Figure 19. Percent of Time with Broken or Overcast Skies and Median Ceiling Heights (in feet) — Whidbey Island, Washington

area just after sunrise in August, maximum heights (5600-foot dashed contour) covering mid-April to mid-July, about one to three hours prior to sunset.

3. SUMMARY

The purpose of the foregoing was to describe and illustrate the use of two-way (hour-month) time-section plots as a means of presenting climatological data, and in the process advance the notion that visual depiction is a more efficient and effective means of conveying the information than, say, tabular summaries. A number of different chart types were presented, based on both originally published and derived climatological parameters.

Depending, of course, on available computing and graphical software resources, visualization charts of these kind are worth considering as planning and decision-making aids for scenarios in which meteorological conditions could have an impact.

4. REFERENCES

- Fisk, C.J., 1999: Feasibility of Generating 24-Hour Mean Vector Wind Statistics From Every-Third-Hour Cross-Tabulated Wind Direction/Speed Data — A Single Station Exploratory Analysis, *Proceedings of the 11th Conference on Applied Climatology*, American Meteorological Society, Dallas.
- Fisk, C.J., 2002: Resultant Wind Constancy and Individual Wind Variability around the Resultant Direction, A Test Analysis Using Point Mugu Data, *Geophysics Branch Technical Note No. 232*. Naval Air Warfare Center, Point Mugu, CA., 8 pp.

Ghosh, J., 2000: *S.B. Devi Charity Home Student s Exchange Proramme to Calcutta. Climate, Geography, Seasons* . 5 pp.
http://www.unibas.ch/calcutta/pdf/sali_neu.pdf

Keislar, R.E., Koracin, D., et.al., 2003: *State Implementation Plan (SIP) Planning Service for the Sacramento Ozone Non-attainment Area , Desert Research Institute, Reno, NV. 28 pp.*
<http://www.airquality.org/cleanairplan/modeling/EpisodeSelection.pdf>

Trewartha, G. T., and Horn, L.H., 1980: *An Introduction to Climate. McGraw-Hill, 416pp.*